Journal of Alloys and Compounds 509 (2011) 8392–8397

Contents lists available at ScienceDirect

Journal of Alloys and Compounds

journal homepage: www.elsevier.com/locate/jallcom

Preparation, structure and electrical conductivity of the pyrochlore-type phase $Sm_2Zr_2O_7$ codoped with bivalent magnesium and trivalent dysprosium cations

Xian-Zhong Xiong, Zhan-Guo Liu, Jia-Hu Ouyang*, Xiao-Liang Xia, Jun Xiang, Xiao-Ming Liu

School of Materials Science and Engineering, Harbin Institute of Technology, 92 West Da-Zhi Street, Harbin 150001, China

ARTICLE INFO

Article history:
Received 3 April 2011
Received in revised form 21 May 2011
Accepted 23 May 2011
Available online 6 June 2011

Keywords:
$SmDy_{1-x}Mg_xZr_2O_{7-x/2}$
Solid electrolyte
Structure
Impedance spectroscopy
Electrical conductivity

ABSTRACT

The pyrochlore-type phases with the compositions of $SmDy_{1-x}Mg_xZr_2O_{7-x/2}$ ($0 \le x \le 0.20$) have been prepared by pressureless-sintering method for the first time as possible solid electrolytes. The structure and electrical conductivity of $SmDy_{1-x}Mg_xZr_2O_{7-x/2}$ ceramics have been studied by the X-ray diffraction (XRD), scanning electron microscopy (SEM) and impedance spectroscopy measurements. $SmDy_{1-x}Mg_xZr_2O_{7-x/2}$ ($x = 0$, 0.05, 0.10) ceramics exhibit a single phase of pyrochlore-type structure, and $SmDy_{1-x}Mg_xZr_2O_{7-x/2}$ ($x = 0.15$, 0.20) ceramics consist of pyrochlore phase and a small amount of the second phase magnesia. The total conductivity of $SmDy_{1-x}Mg_xZr_2O_{7-x/2}$ ceramics obeys the Arrhenius relation, and the total conductivity of each composition increases with increasing temperature from 673 to 1173 K. $SmDy_{1-x}Mg_xZr_2O_{7-x/2}$ ceramics are oxide-ion conductors in the oxygen partial pressure range of 1.0×10^{-4} to 1.0 atm at all test temperature levels. The highest total conductivity value is about 8×10^{-3} S cm^{-1} at 1173 K for $SmDy_{1-x}Mg_xZr_2O_{7-x/2}$ ceramics.

1. Introduction

Solid electrolytes with high oxide-ion conductivity are of considerable scientific interest for their applications in devices such as solid oxide fuel cells (SOFCs), gas sensors, electrochemical sensors, and so on [1–3]. In the present SOFCs system, the state of the art electrolyte material is 8 mol.% yttria-stabilized zirconia (YSZ), and the cathode material is strontium-substituted manganites ($La_{1-x}Sr_xMnO_3$) and the anode material is the Ni–YSZ cermet, respectively [4–6]. However, high operation temperatures promote unwanted reactions in SOFCs, especially at the cathode/electrolyte interface. $La_2Zr_2O_7$ and $SrZrO_3$ resistive layers were reported to form at the interface [7–9]. Both zirconate phases of $La_2Zr_2O_7$ and $SrZrO_3$ lead to an increase in the resistance, and have greatly degraded the performance of SOFCs. In recent years, the challenge of SOFCs technology is to develop practical and cost-effective SOFC systems. As the key part of SOFCs is the solid electrolyte, the research effort mainly focuses on the search for solid electrolytes with a higher oxide-ion conductivity than YSZ [3,10–12].

The $A_2Zr_2O_7$-type (A = lanthanide) pyrochlore oxides have attracted great attention for a long time due to their high-temperature stability and various potential domains of applications such as solid electrolytes, oxygen electrodes, catalysts, thermal barrier coating materials, and so on [13–16]. $A_2Zr_2O_7$-type structure shows the well-known ability of the structure to accommodate oxygen nonstoichiometry. Recently, new $A_2Zr_2O_7$-type oxides are of considerable scientific interests owing to variable cation radius ratios of $r(A^{3+})/r(Zr^{4+})$ and oxygen nonstoichiometry [7,17–21]. The electrical conductivity of the pyrochlore-type $Sm_2Zr_2O_7$ was comparable to those of other oxide-ion conductors in the low-temperature region [17]. At 1023–1173 K, the electrical conductivity of $Sm_2Zr_2O_7$ doped with 2.5–10 mol.% Mg at the Sm site is almost the same as undoped $Sm_2Zr_2O_7$ [18]. For $(Sm_{1-x}Gd_x)_2Zr_2O_7$ ($0 \le x \le 1.0$), $(Sm_{1-x}Y_x)_2Zr_2O_7$ ($0 \le x \le 0.5$) and $(Sm_{1-x}Yb_x)_2Zr_2O_7$ ($0 \le x \le 1.0$) systems, the electrical conductivity of pyrochlore-type compositions is clearly higher than that of defect fluorite-type compositions in the temperature range of 723–1173 K [19–21].

In this work, the pyrochlore-type phase $Sm_2Zr_2O_7$ codoped with magnesium and dysprosium cations, $SmDy_{1-x}Mg_xZr_2O_{7-x/2}$ ($x = 0$, 0.05, 0.10, 0.15, 0.20), were prepared for the first time by pressureless-sintering method at 1973 K for 10 h in air, and the objective of this work is to study the influence of magnesium and dysprosium cations codoping on the structure and electrical conductivity of the pyrochlore-type phase $Sm_2Zr_2O_7$.

2. Experimental procedure

In this study, the pyrochlore series $SmDy_{1-x}Mg_xZr_2O_{7-x/2}$ ($x = 0$, 0.05, 0.10, 0.15, 0.20) were prepared by the solid state reaction method. Appropriate amounts of the relevant oxides, namely Sm_2O_3 (Rare-Chem Hi-Tech Co. Ltd., China; purity ≥ 99.99%), Dy_2O_3 (Rare-Chem Hi-Tech Co. Ltd., China; purity ≥ 99.99%), MgO (Tianjin Hengxing Chemical Preparation Co. Ltd., China; Analytical pure), and ZrO_2 (Dongguan SG Ceramics Technology Co. Ltd., China; purity ≥ 99.9%) powders were

* Corresponding author. Tel.: +86 451 86414291; fax: +86 451 86414291.
E-mail address: ouyangjh@hit.edu.cn (J.-H. Ouyang).

0925-8388/$ – see front matter © 2011 Elsevier B.V. All rights reserved.
doi:10.1016/j.jallcom.2011.05.088

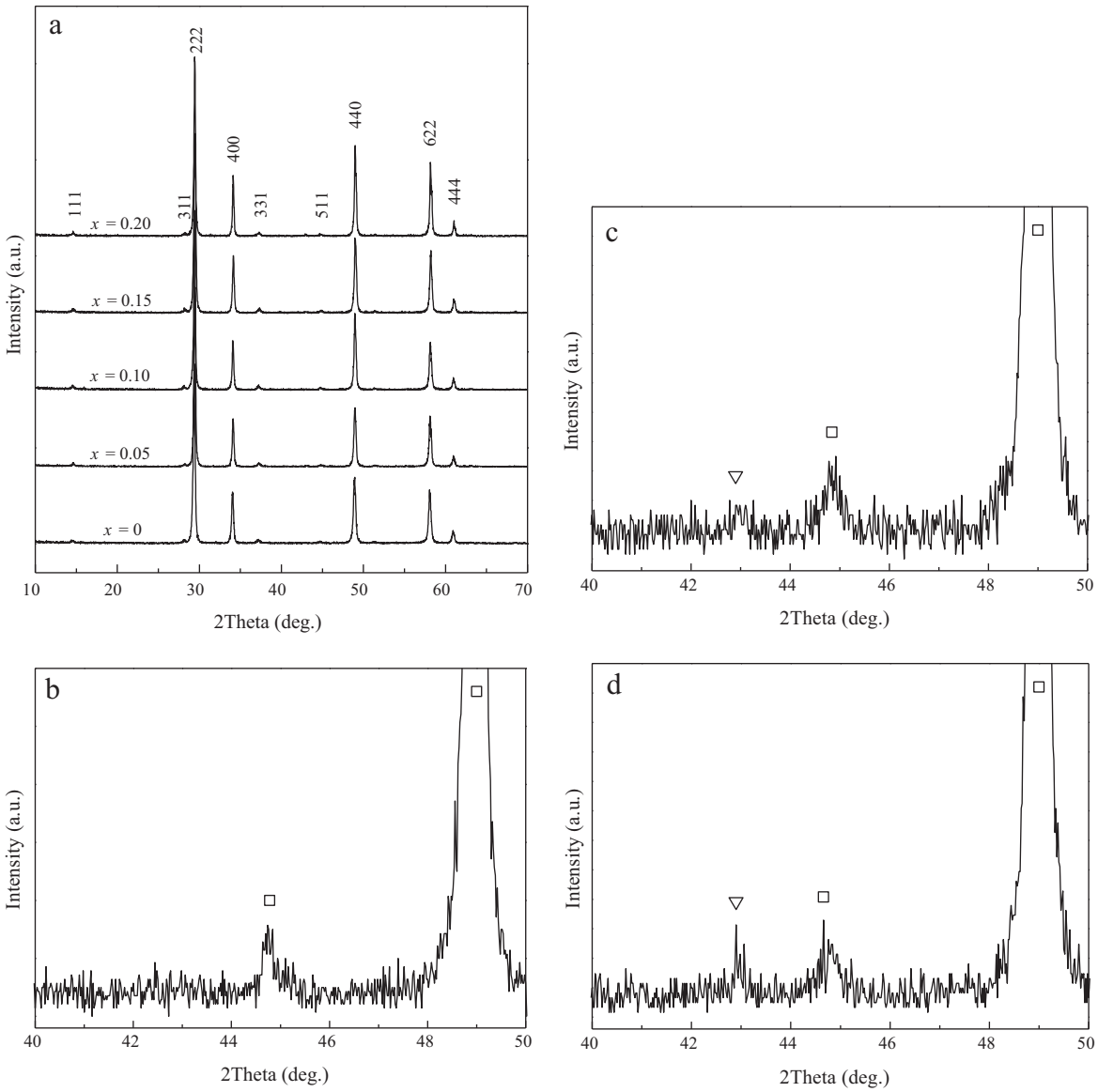

Fig. 1. XRD patterns of $SmDy_{1-x}Mg_xZr_2O_{7-x/2}$ ceramics sintered at 1973 K for 10 h in air: (a) 2θ range of 10°–70°, (b–d) 2θ range of 40°–50° for $x = 0.10$, 0.15 and 0.20, respectively (▽ – MgO, □ – pyrochlore).

homogenized using zirconia balls and analytically pure alcohol. All oxide powders were calcined at 1173 K for 2 h in air prior to mixing. The powder mixtures were uniaxially pressed into pellets at 20 MPa, subsequently cold isostatically pressed at 400 MPa for 5 min, and then pressureless-sintered at 1973 K for 10 h in air.

The phase structure of the sintered ceramics was identified by X-ray diffractometry (XRD). XRD data were collected on a diffractometer (Rigaku D/Max 2200VPC, Japan) using Cu $K\alpha$ radiation (40 kV, 30 mA) in a 2θ range from 10° to 70° at room temperature. XRD patterns were recorded in a continuous scan mode with a scan rate of 4°/min. The apparent density of sintered pellets was determined by the usual volume and weight measurement technique. The microstructures of the sintered ceramics were characterized with a scanning electron microscope (FEI Quanta 200F, the Netherlands), while the local compositions of interest were particularly analyzed with the equipped energy-dispersive X-ray spectroscopy. SEM specimens were prepared by polishing the surface to 1 μm finish, and then by thermally etching at 1873 K for 1 h in air. A thin carbon coating was evaporated onto the surfaces of the specimens for SEM observations.

Impedance spectroscopy data were collected in air using an impedance/gain-phase analyzer (Solartron™ SI 1260, UK). The applied stimulus amplitude in the AC impedance measurements was 20 mV and the frequency range was 0.2 Hz–2 MHz. For impedance measurements, the dimensions of the samples were about 8 mm in diameter and 1 mm in thickness. Electrodes were prepared by coating both pellet faces with a platinum paste, which were then heated at 1223 K for 2 h in air to decompose the paste and harden the Pt residue. Platinum wires were attached to the surface of the samples for measurements. Data are recorded over the temperature range of 673–1173 K in a 50 K interval during heating with an equilibration time of at least 30 min. The impedance measurements as a function of oxygen partial pressure were performed in a closed tube furnace cell. The oxygen partial pressure $p(O_2)$ ranged from around 1.0×10^{-4} to 1.0 atm, and was monitored by a YSZ sensor. The process involved flushing the system with a N_2–O_2 gas mixture. Zview 3.1c software was used to analyze all the impedance data.

3. Results and discussion

XRD patterns of the as-prepared $SmDy_{1-x}Mg_xZr_2O_{7-x/2}$ ceramics sintered at 1973 K for 10 h in air are shown in Fig. 1. It can be seen that $SmDy_{1-x}Mg_xZr_2O_{7-x/2}$ ($x = 0$, 0.05, 0.10) crystallize with a pyrochlore-type structure that can be described in standard cubic space group F$d3m$ (no. 227). When the Sm^{3+} is partially substituted by Mg^{2+} and Dy^{3+} with different concentrations, XRD patterns show impurity phase peaks, as shown in Fig. 1(c) and (d). $SmDy_{1-x}Mg_xZr_2O_{7-x/2}$ ($x = 0.15$, 0.20) consist of the pyrochlore-type structure and a small amount of magnesia. Typical SEM micrographs of $SmDy_{1-x}Mg_xZr_2O_{7-x/2}$ ceramics are displayed in Fig. 2. From SEM images, pores in as-sintered ceramics become less and less with increasing magnesium content. The grains are nearly uniform and similar for each composition,

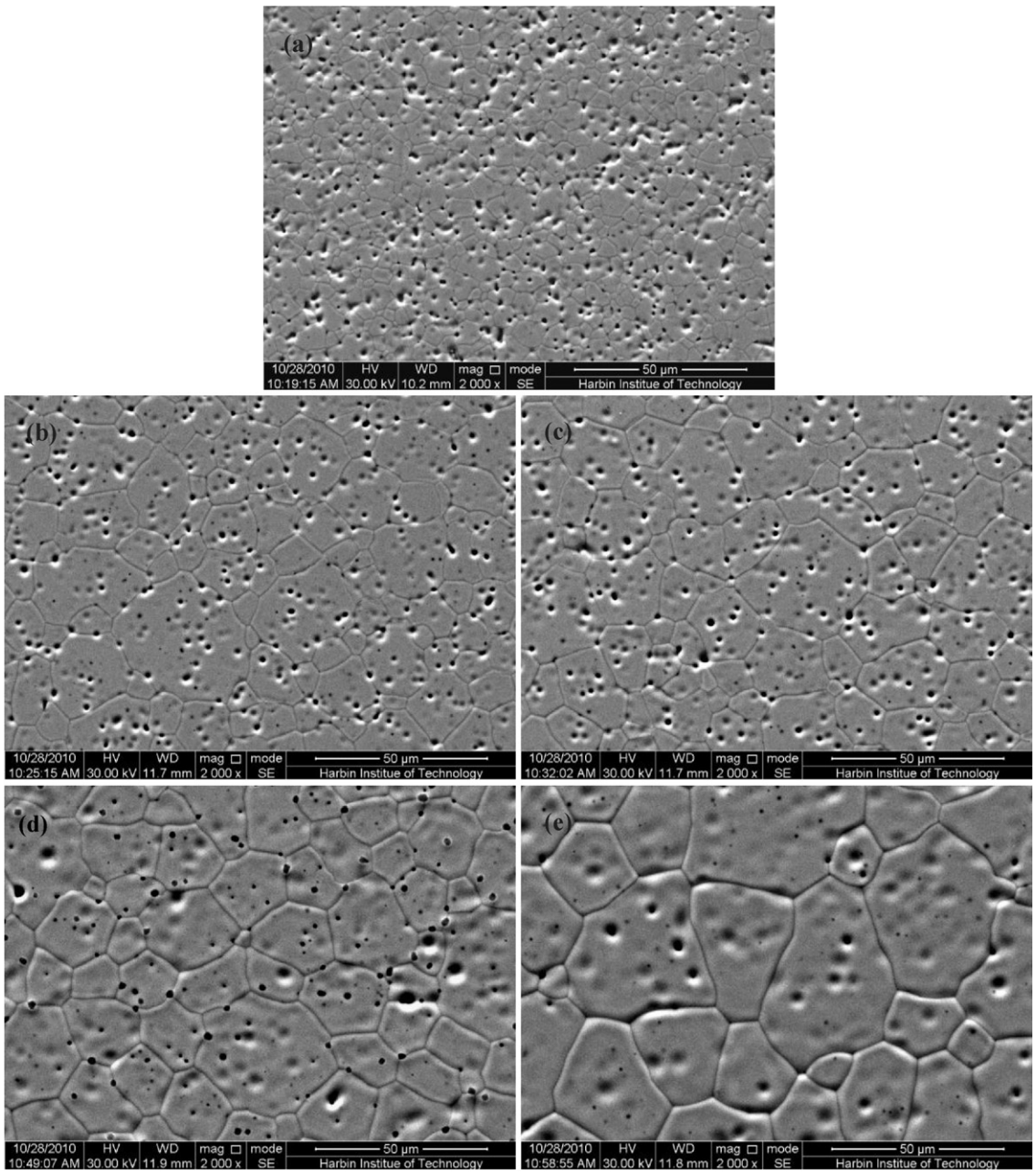

Fig. 2. SEM micrographs of the thermally etched surface of $SmDy_{1-x}Mg_xZr_2O_{7-x/2}$ ceramics: (a) $x = 0$, (b) $x = 0.05$, (c) $x = 0.10$, (d) $x = 0.15$, (e) $x = 0.20$.

and the grain boundaries are very clean. Clearly, the average grain size of $SmDy_{1-x}Mg_xZr_2O_{7-x/2}$ ceramics gradually increases with increasing magnesium content. From Fig. 2(d) and (e), the second phase can be clearly observed as contrasted with the results in Fig. 2(a)–(c). Fig. 3(a) and (b) shows the secondary electron image and the corresponding backscattered electron image of the $SmDy_{0.85}Mg_{0.15}Zr_2O_{6.925}$ ceramic. It is clearly seen that the $SmDy_{0.85}Mg_{0.15}Zr_2O_{6.925}$ ceramic is composed of two phases. The EDS spectra obtained at different positions of A and B in Fig. 3(a) confirmed the presence of the pyrochlore-type phase (position A) and magnesia phase (position B), as shown in Fig. 3(c) and (d). The relative densities of $SmDy_{1-x}Mg_xZr_2O_{7-x/2}$ ($x = 0$, 0.05, 0.10) ceramics are 94.7%, 97.1% and 97.2%, respectively. $SmDy_{1-x}Mg_xZr_2O_{7-x/2}$ ($x = 0.15$, 0.20) ceramics have a higher relative density than $SmDy_{1-x}Mg_xZr_2O_{7-x/2}$ ($x = 0$, 0.05, 0.10), which is consistent with SEM observations. It indicates that magnesia can promote the sintering densification behavior of zirconate ceramics.

Fig. 4(a)–(e) presents a series of representative impedance spectra of measured (squares) data for $SmDy_{1-x}Mg_xZr_2O_{7-x/2}$ ceramics, which were obtained at 673 K in air. The impedance spectra were fitted using equivalent circuits consisting of a serial association of (RC) elements ascribed to electrolyte or electrode processes, where R is a resistance and C is a constant phase element in parallel. From Fig. 4(a)–(e), three distinct contributions are observed, and therefore the following equivalent circuit was considered for the fitting [22–24]: $(RC)_G(RC)_{GB}(RC)_E$, where the subscripts G and GB represent the grain and grain-boundary contributions of the electrolyte, respectively, and E is the electrode process, as shown in Fig. 4(f). The grain resistance (R_G) and capacitance (C_G), and the grain-boundary resistance (R_{GB}) and capacitance (C_{GB}) of the electrolyte can be obtained in this way. From fitted results, at 673 K, the capacitance for the high frequency arc is determined to be in the order of pF, the intermediate frequency arc shows capacitance in the order of nF, and the low frequency arc exhibits capacitance

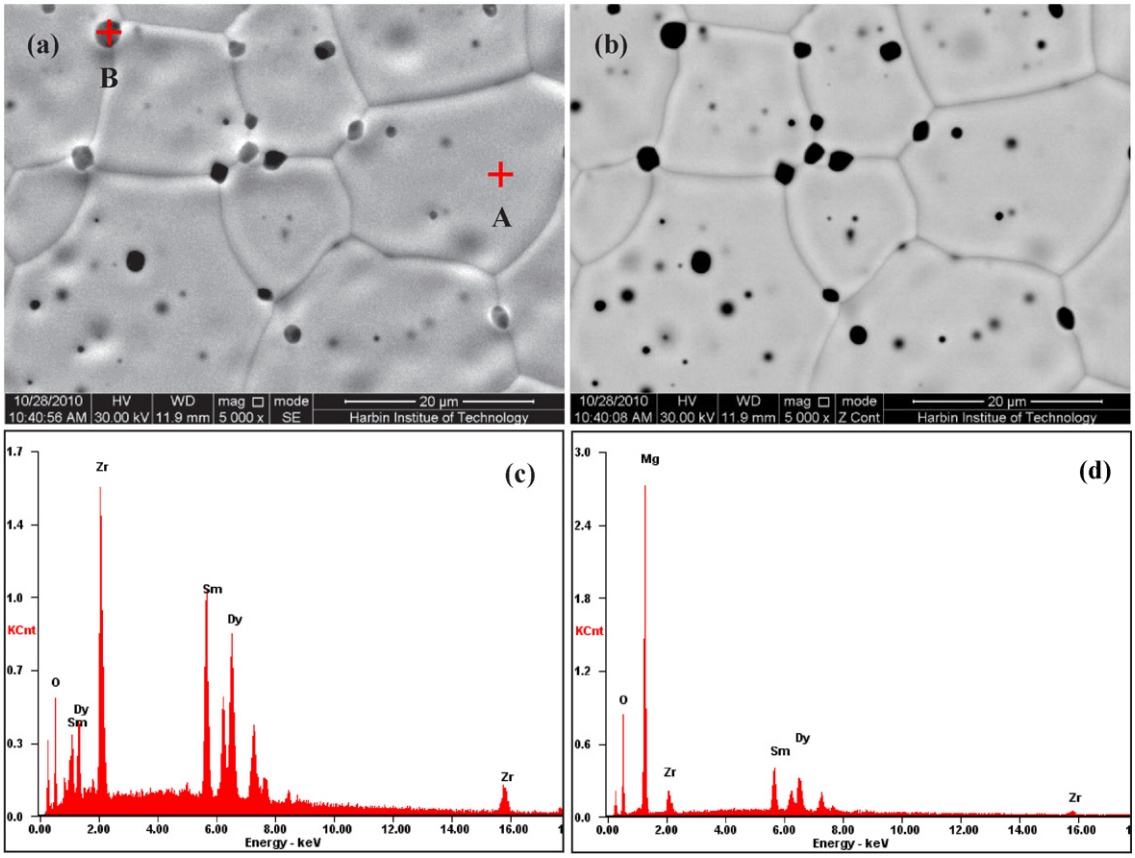

Fig. 3. Microstructure of $SmDy_{0.85}Mg_{0.15}Zr_2O_{6.925}$ ceramic: (a) secondary electron image, (b) corresponding backscattered electron image; (c) and (d) EDS spectra at the positions of A and B in (a), respectively.

in the order of μF. These are typical values for the grain, grain-boundary, and electrode contributions in the solid electrolyte [25]. In order to better understand the influence of magnesium and dysprosium cations codoping on the total conductivity of the $Sm_2Zr_2O_7$ pyrochlore, the intermediate frequency intercept to the Z' axis is considered to determine the total resistance ($R_G + R_{GB}$). In practice, the total conductivity may be more relevant as compared with the grain or grain-boundary conductivity. The total conductivity of $SmDy_{1-x}Mg_xZr_2O_{7-x/2}$ ceramics at different temperatures can be obtained using the following equation:

$$\sigma = \frac{L}{S \cdot R_T} \quad (1)$$

where L and S denote the sample thickness and the electrode area of the sample surface, respectively, and $R_T = R_G + R_{GB}$.

The temperature dependence of the total conductivity of $SmDy_{1-x}Mg_xZr_2O_{7-x/2}$ ceramics in air is shown in Fig. 5, which is obtained from the impedance spectra over the temperature range of 673–1173 K. The temperature dependence of the total conductivity could be described by the Arrhenius equation with the following expression:

$$\sigma \cdot T = \sigma_0 \exp\left(\frac{-E}{k_B T}\right) \quad (2)$$

where σ, T, σ_0, E and k_B are the total conductivity, absolute temperature, pre-exponential factor, activation energy and Boltzman constant, respectively. The total conductivity data follow the linear behavior, which confirms that the ionic diffusion process is thermally activated. For each composition, the activation energy and pre-exponential factor are calculated from the slope and the intercept of the linear fits in the Arrhenius plots (Fig. 5), respectively. The latter is indicative of the number of charge carriers available for conduction [26–28]. The calculated values of the activation energy and pre-exponential factor are presented in Table 1. The activation energy for the total conductivity of $SmDy_{1-x}Mg_xZr_2O_{7-x/2}$ ceramics is in the range of 1.059–1.259 eV.

Fig. 6 shows the variations in the total conductivity of $SmDy_{1-x}Mg_xZr_2O_{7-x/2}$ ceramics as a function of magnesium content at different temperatures. It is evident that the total conductivity of each composition gradually increases with increasing temperature from 673 to 1173 K. With the increase of magnesium content, the total conductivity of $SmDy_{1-x}Mg_xZr_2O_{7-x/2}$ ceramics slightly decreases from $x = 0$ to $x = 0.20$. At 1073–1173 K, various compositions of $SmDy_{1-x}Mg_xZr_2O_{7-x/2}$ ceramics have a similar value of the total conductivity. The highest total conductivity value is about 8×10^{-3} S cm^{-1} at 1173 K for $SmDy_{1-x}Mg_xZr_2O_{7-x/2}$ ceramics. The oxygen partial pressure $p(O_2)$ dependence of the total conductivity was measured for $SmDy_{1-x}Mg_xZr_2O_{7-x/2}$ ceramics in order to clarify conduction carrier. Fig. 7 shows the total conductivity of the $SmDy_{0.9}Mg_{0.1}Zr_2O_{6.95}$ ceramic as a function

Table 1
Activation energy and pre-exponential factor for the total conductivity of $SmDy_{1-x}Mg_xZr_2O_{7-x/2}$ ceramics.

Magnesium content (x) in $SmDy_{1-x}Mg_xZr_2O_{7-x/2}$	Activation energy E (eV)	Pre-exponential factor σ_0 (S cm^{-1} K)
0	1.059	4.122×10^5
0.05	1.104	6.313×10^5
0.10	1.210	1.887×10^6
0.15	1.197	1.618×10^6
0.20	1.259	2.921×10^6

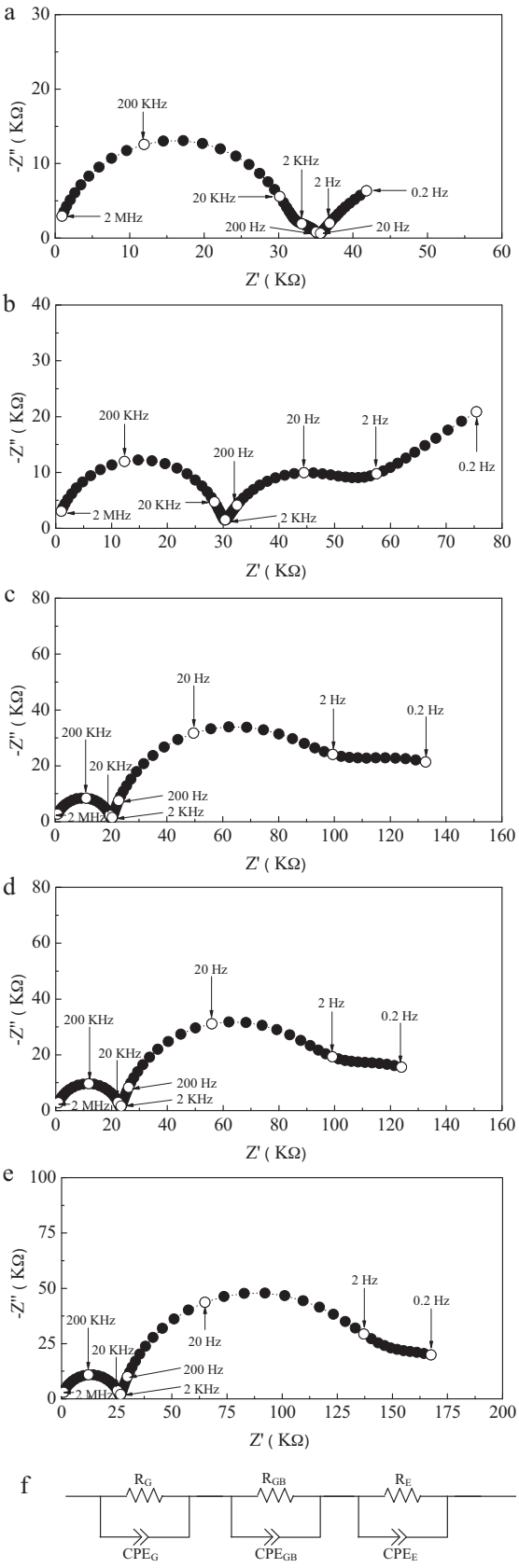

Fig. 4. Impedance spectra and schematic equivalent electrical circuit plots of $SmDy_{1-x}Mg_xZr_2O_{7-x/2}$ ceramics at 673 K in air: (a) $x = 0$, (b) $x = 0.05$, (c) $x = 0.10$, (d) $x = 0.15$, (e) $x = 0.20$, (f) equivalent electrical circuit.

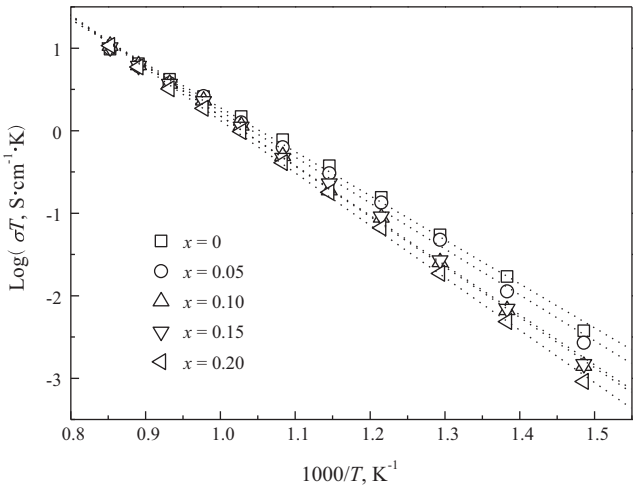

Fig. 5. Arrhenius plots of the total conductivity of $SmDy_{1-x}Mg_xZr_2O_{7-x/2}$ ceramics.

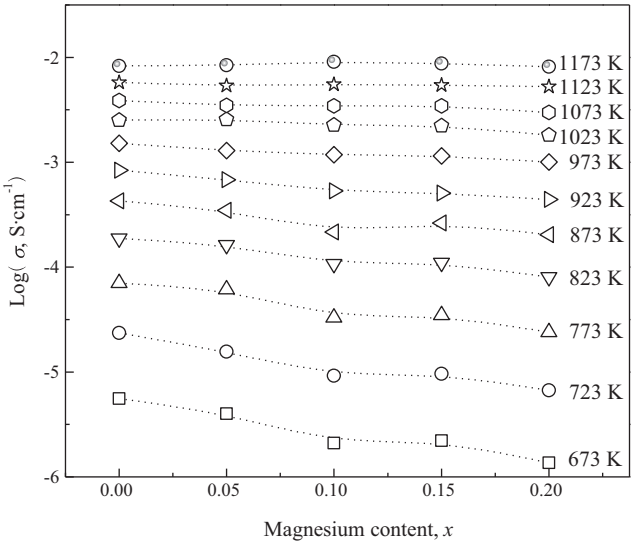

Fig. 6. Compositional dependence of the total conductivity of $SmDy_{1-x}Mg_xZr_2O_{7-x/2}$ ceramics as a function of magnesium content.

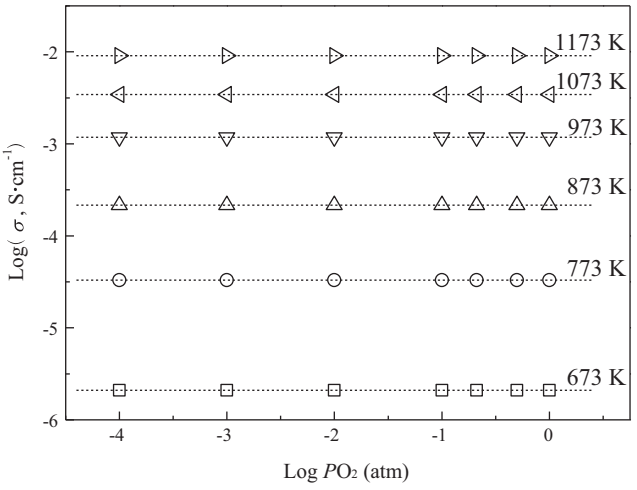

Fig. 7. Oxygen partial pressure dependence of the total conductivity of $SmDy_{1-x}Mg_xZr_2O_{7-x/2}$ ($x = 0.10$) ceramic.

of oxygen partial pressure at different temperatures, which was calculated from the impedance spectra. Clearly, the total conductivity of the $SmDy_{0.9}Mg_{0.1}Zr_2O_{6.95}$ ceramic is almost independent of oxygen partial pressure from 1.0×10^{-4} to 1.0 atm at all test temperature levels, respectively, which indicates that the conduction is purely ionic conductivity and does not contain any electronic conduction [29]. In consideration of the total conductivity of the $SmDy_{1-x}Mg_xZr_2O_{7-x/2}$ ceramics, which is slightly lower than that of conventional solid electrolytes such as YSZ (1×10^{-2} S cm^{-1}, 973 K [30]), the most likely applications of $SmDy_{1-x}Mg_xZr_2O_{7-x/2}$ ceramics in SOFCs are high-temperature solid electrolytes, or thick-film electrolytes, or as protective layers applied onto CeO_2- or $LaGaO_3$-based solid electrolytes [31].

4. Conclusions

$SmDy_{1-x}Mg_xZr_2O_{7-x/2}$ (x = 0, 0.05, 0.10) ceramics exhibit a single phase of pyrochlore-type structure, and $SmDy_{1-x}Mg_xZr_2O_{7-x/2}$ (x = 0.15, 0.20) ceramics are composed of pyrochlore phase and a small amount of the second phase magnesia. The relative density of $SmDy_{1-x}Mg_xZr_2O_{7-x/2}$ ceramics is in the range of 94.7–99.8%. The total conductivity of $SmDy_{1-x}Mg_xZr_2O_{7-x/2}$ ceramics obeys the Arrhenius relation, and the total conductivity of each composition increases with increasing temperature from 673 to 1173 K. $SmDy_{1-x}Mg_xZr_2O_{7-x/2}$ ceramics are oxide-ion conductors in the oxygen partial pressure range of 1.0×10^{-4} to 1.0 atm at all test temperature levels. The highest total conductivity value is about 8×10^{-3} S cm^{-1} at 1173 K for $SmDy_{1-x}Mg_xZr_2O_{7-x/2}$ ceramics.

Acknowledgements

This work was financially supported by the National Natural Science Foundation of China (NSFC, Grant Nos. 50972030 and 51021002), and the Fundamental Research Funds for the Central Universities (Grant No. HIT.BRET1.2010006).

References

[1] D.J.L. Brett, A. Atkinson, N.P. Brandon, S.J. Skinner, Chem. Soc. Rev. 37 (2008) 1568–1578.
[2] M.C. Tucker, J. Power Sources 195 (2010) 4570–4582.
[3] D.F. Wang, J.X. Wang, C.R. He, Y.K. Tao, C. Xu, W.G. Wang, J. Alloys Compd. 505 (2010) 118–124.
[4] J. Malzbender, R.W. Steinbrech, L. Singheiser, Fuel Cells 9 (2009) 785–793.
[5] T.S. Li, W.G. Wang, H. Miao, T. Chen, C. Xu, J. Alloys Compd. 495 (2010) 138–143.
[6] X.B. Zhu, Z. Lu, B. Wei, M.L. Liu, X.Q. Huang, W.H. Su, Electrochim. Acta 55 (2010) 3932–3938.
[7] J.A. Díaz-Guillén, A.F. Fuentes, M.R. Díaz-Guillén, J.M. Almanza, J. Santamaría, C. León, J. Power Sources 186 (2009) 349–352.
[8] M. Chen, Y.-L. Liu, A. Hagen, P.V. Hendriksen, F.W. Poulsen, Fuel Cells 9 (2009) 833–840.
[9] C. Levy, Y. Zhong, C. Morel, S. Marlin, J. Electrochem. Soc. 157 (2010) B1597–B1601.
[10] S.P. Jiang, L. Zhang, H.Q. He, R.K. Yap, Y. Xiang, J. Power Sources 189 (2009) 972–981.
[11] Z.-G. Liu, J.-H. Ouyang, K.-N. Sun, X.-L. Xia, Electrochim. Acta 55 (2010) 8466–8470.
[12] L.D. Jadhav, M.G. Chourashiya, A.P. Jamale, A.U. Chavan, S.P. Patil, J. Alloys Compd. 506 (2010) 739–744.
[13] M.A. Subramanian, G. Aravamudan, G.V. Subba Rao, Prog. Solid State Chem. 15 (1983) 55–143.
[14] J. Cheng, J.J. Li, C.Y. Ma, Z.P. Hao, Catal. Commun. 10 (2009) 1170–1173.
[15] Z.-G. Liu, J.-H. Ouyang, Y. Zhou, J. Alloys Compd. 472 (2009) 319–324.
[16] Z.H. Xu, L.M. He, R.D. Mu, S.M. He, G.H. Huang, X.Q. Cao, J. Alloys Compd. 504 (2010) 382–385.
[17] K. Shinozaki, M. Miyauchi, K. Kuroda, O. Sakurai, N. Mizutani, M. Kato, J. Am. Ceram. Soc. 62 (1979) 538–539.
[18] X.-L. Xia, J.-H. Ouyang, Z.-G. Liu, S. Li, Sci. Adv. Mater. 2 (2010) 497–502.
[19] Z.-G. Liu, J.-H. Ouyang, Y. Zhou, X.-L. Xia, J. Power Sources 185 (2008) 876–880.
[20] X.-L. Xia, J.-H. Ouyang, Z.-G. Liu, S. Gao, S. Li, J. Electrochem. Soc. 157 (2010) B470–B476.
[21] Z.-G. Liu, J.-H. Ouyang, Y. Zhou, X.-L. Xia, Electrochim. Acta 54 (2009) 3968–3971.
[22] J.R. Macdonald, W.B. Johnson, Impedance Spectroscopy: Theory, in: E. Barsoukov, J.R. Macdonald (Eds.), Experiment and Applications, 2nd Ed., John Wiley & Sons, Inc., New Jersey, 2005, Chapter 1.
[23] B. Rangarajan, S.S.N. Bharadwaja, E. Furman, T. Shrout, M. Lanagan, J. Am. Ceram. Soc. 93 (2010) 522–530.
[24] T.P. Holme, R. Pornprasertsuk, F.B. Prinz, J. Electrochem. Soc. 157 (2010) B64–B70.
[25] Q. Li, V. Thangadurai, Fuel Cells 9 (2009) 684–698.
[26] H. Yamamura, H. Nishino, K. Kakinuma, K. Nomura, Solid State Ionics 158 (2003) 359–365.
[27] J.A. Díaz-Guillén, M.R. Díaz-Guillén, K.P. Padmasree, A.F. Fuentes, J. Santamaría, C. León, Solid State Ionics 179 (2008) 2160–2164.
[28] A.N. Radhakrishnan, P.P. Rao, K.S.M. Linsa, M. Deepa, P. Koshy, Dalton Trans. 40 (2011) 3839–3848.
[29] J.B. Goodenough, Annu. Rev. Mater. Res. 33 (2003) 91–128.
[30] A.J. Jacobson, Chem. Mater. 22 (2010) 660–674.
[31] V.V. Kharton, F.M.B. Marques, A. Atkinson, Solid State Ionics 174 (2004) 135–149.